Indian Journal of Geo Marine Sciences
Vol. 49 (02), February 2020, pp. 225-232

Antarctic snowmelt detection for QuikSCAT scatterometer data based on mathematical morphology combined with wavelet transform

Xingdong Wang* & Shuo Liu

College of Information Science and Engineering, Henan University of Technology, Zhengzhou, Henan, China

*[E-mail: zkywxd@163.com]

Received 26 July 2018; revised 01 October 2018

Microwave scatterometer is sensitive to the melting snow. When the freeze-thaw phenomenon occurs, the backscatter coefficients will have a sharp rising and falling mutation. Mathematical morphology has the characteristics with edge-preserving filter and wavelet transform has the characteristics with the automatic edge extraction, which does not depend on the priori snowmelt information. A new automatic Antarctic snowmelt detection method was proposed based on mathematical morphology combined with wavelet transform. This method improves the snowmelt detection accuracy, because this method can remove the interference of the edge extraction. Melt onset date, end date and duration can be obtained with high accuracy by identifying and tracking the sharp rising and falling edge. Compare the snowmelt results in this work with the temperature of ten automatic weather stations (AWS), which shows that the snowmelt detection method proposed in the paper improves the detection accuracy from about 50 % to 62.5 % in AWS Cape Denison.

[**Keywords:** Generalized Gaussian model; Mathematical morphology; Microwave scatterometer; Snowmelt detection; Wavelet transform]

Introduction

Antarctica plays an important role in the global heat budget. As one of the main sources of cold air on the Earth, Antarctica has a profound impact on global climate. Ice sheet is one of the most important environmental factors in Antarctica, and changes in ice sheet play an important role in regulating the global climate. The near-surface snowmelt in Antarctica will cause the increase of the surface humidity, leading to the collapse of the ice shelves, sea level rise[1], and then it will change the movement of the ice streams, and also change the radiation reflectivity of the snow and thus affecting the polar radiation balance. Therefore, the polar snowmelt could serve both as a sensitive indicator and a strong contributing factor to global climate change[2-3]. So accurately and objectively detecting melt onset date, end date, and duration of the snow has important theoretical significance and practical application value.

The QuikSCAT scatterometer has the widely spatial coverage and daily time resolution, and it is not affected by weather and night and has high sensitivity, which provides an ideal tool for the seasonal snowmelt detection over Antarctica[4]. When the liquid water content of snow increases, there is a sudden decrease in the backscatter values from the QuikSCAT scatterometer[5-7], and this property has been successfully used for the detection of polar ice-sheet and the ice-shelf melt onset date[4,8,9]. The sharp decline time of the backscatter coefficient is consistent with the air temperature more than 0 °C and this phenomenon can be used for snowmelt detection[8,10]. In the melt season, due to the increase of microwave absorption, the decrease of backscatter coefficient (radar cross section σ^0) is dramatic such that this phenomenon can be easily used to detect the snowmelt. For example, microwave scatterometer data has been successfully used in Arctic to recognize the thaw-freeze information of snow and ice[11], which has been successfully applied to the ice-sheet melt area and the duration map in Greenland[12], and estimate the snow and ice-sheet accumulation of Greenland island[13], and determine the Arctic melting / freezing onset date[13-14].

There are the following several kinds of methods of ice-sheet freeze-thaw detection for the microwave scatterometer: (1) The threshold-based ice-sheet freeze-thaw detection methods[6,15-18]: Ashcraft and Long[16] used the mean and standard deviation of the backscatter coefficient during the winter where a drop in the backscatter coefficient of eight winter standard deviations below the winter mean indicates a melt.

Nghiem et al.[17] used QSCAT to detect melt over Greenland based on the diurnal variability. Ashcraft and Long[16] used a threshold of 3 dB below the winter mean. Bartsch et al.[18] presented an approach for monitoring of differences in backscatter measured during morning and evening passes. Bothale et al.[6] presented a threshold method based on temperature HH polarized backscatter coefficient relation and average HH polarized backscatter coefficient for the months January-March used for melt/freeze detection in Himalaya. Bothale et al.[7] presented an adaptive threshold-based classification for melt/freeze detection using austral winter mean and standard deviation. (2) The model-based ice-sheet freeze-thaw detection methods: it mainly includes $Q-\alpha$ method of QuickSCAT scatterometer and $E-\alpha$ method of ERS scatterometer[15]. (3) The improved methods are based on the former two methods[11,12,19]. The typical ice-sheet freeze-thaw detection methods are based on the averages of the backscatter coefficients for 5 days in a row, and three-step method is based on the change of the backscatter coefficient in a day, as well as the method of dynamic threshold value and the method of dual threshold values and so on. (4) The ice-sheet freeze-thaw detection methods based on edge detection: Steiner and Tedesco[8] proposed wavelet-based melt algorithm based on wavelets and multiscale analysis. The advantage of this method is that it does not depend on the field measurements, which depend only on the relative backscatter values. The disadvantage is that the mutation is not very ideal, and the typical sample of the double Gauss model is time-consuming.

Microwave scatterometer has high sensitivity and the roughness has a greater influence on the backscatter coefficient, and the surface roughness of the wet snow is generally greater than the dry snow, therefore, the backscatter coefficient of the wet snow is very sensitive to the surface roughness. In order to get accurate melt information by wavelet edge detection method, there is a need to remove the interference of the surface roughness of the wet snow. The introduced mathematical morphology is not only able to filter out the interference effectively but also can well keep the edge information.

Materials and Methods

Materials

The scattermeter SeaWinds / QSCAT was launched in 1999 with QuikSCAT satellite, and its working frequency is 13.4 GHz using a conical scanning pen type antenna. Internal and external beams of QSCAT use two fixed incident angle (46° and 54°) and corresponding HH (horizontal polarization) mode and VV (vertical polarization) mode. This paper mainly uses the spatial resolution $4.45\text{km}\times 4.45\text{km}$ data with SIR (Scatterometer Image Reconstruction) format. This file is composed of the file header and the data subject, and the size of the file header is 512 bytes, which contains the data subject information and projection information.

Both every 3-hour temperature data and every 10-minute temperature data can be used in Antarctica. Because the every 3-hour temperature data has been calibrated and the erroneous data has been removed, we use every 3-hour temperature data to verify the results. The mean value of the daily maximum three data is used as the verification for Antarctic snowmelt results.

Methods

Mathematical morphology

Mathematical morphology is a new image analytical science, and it is the mathematical foundation of integral geometry and random-set theory. Mathematical morphology is a nonlinear filtering method in signal processing, and it is not sensitive to image edge direction, and it can restrain the noise well and keep the real edge. Mathematical morphology is initially targeted at the two-value image operation, because it can not only simplify the image data and keep the basic shape characteristics of the image but also can remove the irrelevant structure in the image, so it is widely applied in the fields of image processing.

Mathematical morphology detects the signal through constantly moving the structure element 'probe', and then the complex signals will be decomposed into many parts with the physical meaning, and the main characteristics of the signal are retained in order to achieve the purpose of extracting useful information. It mainly includes four kinds of basic operations, including corrosion, expansion, opening operation and closing operation.

The set A is corroded by the set B expressed as $A\Theta B$, which is defined as:

$$A\Theta B = \{x : B + x \subset A\} \quad \ldots(1)$$

Where, A is the input image, B is the structure element. $A\Theta B$ is composed of all the points x still included in A by B translating x unit.

Dilation operation and corrosion operation are dual, so it can be defined by the complementary set of the corrosion. A^c expresses the complement set of A, and then the set A expanded by the set B is defined as:

$$A \oplus B = \{A^c \Theta (-B)^c\} \quad \ldots(2)$$

A is the input image, and B is the structure element. The opening operation A done by B is defined as:

$$A \circ B = (A \Theta B) \oplus B \quad \ldots(3)$$

From equation (3) it shows that opening operation is the result that actually A is corroded first, and then it is expanded by B.

Closing operation is the dual operation of the opening operation, first expansion and then corrosion, which is defined as:

$$A \bullet B = (A \oplus B) \Theta B \quad \ldots(4)$$

The opening operation and the closing operation of the mathematical morphology have the low-pass filter characteristics. The opening operation can remove the burrs and the tiny spots of the signal to suppress the peak (positive impulse) noise in the signal, and the closing operation can fill the gaps and the cracks to suppress the (negative pulse) noise in the signal. These operators and their combination can do image segmentation, feature extraction and edge detection.

Multiscale edge detection based on wavelet transform

Because the large number of edges are not differentiable and even not continuous, most of the multiscale edge detections are to smooth the original signals in different scale, and then detect the upheaval point by the first derivative or the second derivative of the smoothed signals, and that is the signal edge.

Let $\theta(x)$ as the smooth function with $\theta(x) = O(1/(1+x^2))$ and $\int_{-\infty}^{+\infty} \theta(t)\, dt \neq 0$. Let $\theta_s(x) = (1/s)\theta(x/s)$ as the upheaval points of the function $f(x)$ smoothed by $\theta_s(x)$ in scale s.

Wavelets $\psi^1(x)$ and $\psi^2(x)$ are defined by the following two formulas separately $\psi^1(x) = \dfrac{d\theta(x)}{dx}$ and $\psi^2(x) = \dfrac{d^2\theta(x)}{dx^2}$, and the corresponding wavelet transform is defined for $W^1 f(\mu, s) = f(x) * \psi^1(x)$ and $W^2 f(\mu, s) = f(x) * \psi^2(x)$, that is:

$$W^2 f(\mu(\mu = f * (s^2 \frac{d^2\theta_s}{dx^2})(x) = s^2 \frac{d^2}{dx^2}(f * \theta_s)(x) \quad \ldots(5)$$

$$W^1 f(\mu, s) = f * (s \frac{d\ \theta_s}{dx})(x) = s \frac{d}{dx}(f * \theta_s)(x) \quad \ldots(6)$$

It can been seen from formula (5) and formula (6) that the wavelet transform of $\psi^1(x)$ and $\psi^2(x)$ for $f(x)$ becomes the convolution with the smooth function $\theta_s(x)$ for one order derivative and two order derivative multiplied by s and s^2. In this way, the local maximization of $\psi^1(x)$ is corresponding to zero point and inflection point of $\psi^2(x)$.

Detecting the zero point or the local extremum point uses the similar method, but the local extreme point has its advantages. The inflection point of $f * \theta_S$ is the maximum point and minimum point of the absolute value of the first derivative, and the maximum point of the first derivative of $f * \theta_s$ is its upheaval points, and the minimum point is its slow change point. It is different to distinguish the maximum point and minimum point by the zero points of the second derivative. But the upheaval point and the value can been obtained easily by detecting the local maximum values of $W^1 f(\mu, s)$, and it plays a very good deionising effect through the screening these local maximum points.

It can been seen that the large-scale wavelet decomposition compared to the small-scale wavelet decomposition not only retains the information of the dramatic changing edge, but also has a certain denoising effect from the multi-scale wavelet decomposition.

Mathematical morphology combined with wavelet transform

Daily backscatter coefficient (σ^0) variations for typical wet and dry pixels are displayed for the horizontal polarization QuikSCAT data from July 1, 2000 to June 30, 2001 as shown in Figure 1. The wet pixel and the dry pixel are filtered by mathematical morphology with edge preserving properties. The dry pixel (80.07˚S, 45.00˚E) is located in the interior of Antarctica, where the ice sheet remained continuously dry and the backscatter coefficient varied smoothly. The wet snow pixel (68.00˚S, 61.18˚W) is located in Larsen ice shelf of Antarctic Peninsula, where the ice sheet experienced melting during the austral summer. The most prominent feature of the wet snow pixel is that its backscatter coefficient decreased rapidly at the

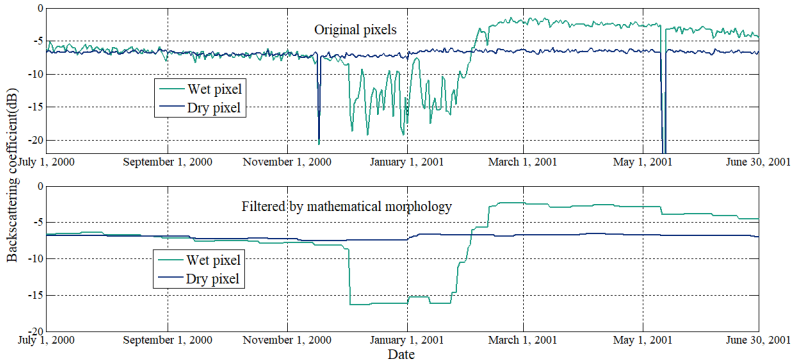

Fig. 1 — Daily backscatter coefficient variations for typical wet and dry pixels

melt onset date in early summer. This stands in sharp contrast to the upper σ^0 observed during the nonmelt conditions, forming a strong downward step edge (cliff) on the time series of daily σ^0 observations. An apparent prolonged period (plateau) of elevated backscatter coefficients is observed during the summer. A dramatic increase in backscatter coefficients corresponding to the snow refreezing creates an obvious upward edge (cliff) on the σ^0 time series curve during the late summer. The basic steps of the filter for the long time series of backscatter coefficient data by mathematical morphology are as follows: 1) The backscatter coefficient data of microwave scatterometer is pre-processed. 2) The opening operation of mathematical morphology does the filter for the long time series of backscatter coefficient data. 3) The closing operation of mathematical morphology does the filter for the results proposed by step 2). It can been seen from the front depiction that the backscatter coefficient changes of the wet snow pixel are mainly determined by the liquid water content in the wet snow. With the increase of the liquid water content in the wet snow in summer, the long time series of backscatter coefficient data has a distinct falling edge filtered by mathematical morphology, which indicates that the ice sheet is melting[20,22].

Based on the above theory, Figure 2 shows Antarctic ice-sheet freeze-thaw detection basic flow chart based on mathematical morphology with wavelet edge detection for microwave scatterometer. The basic principle is as follows: mathematical morphology filters the long time series of backscatter coefficient data with edge preserving, and the sharp falling edge in the curve reacts the ice-sheet melt, and the sharp rising edge in the curve reacts the ice sheet from the melt to the freezing. The melt onset date in every year is the first sharp falling

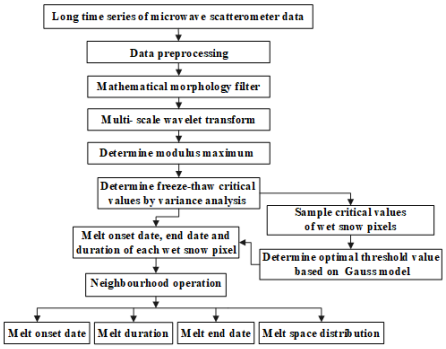

Fig. 2 — Freeze-thaw flowchart of mathematical morphology combined with wavelet transform

edge for the backscatter coefficient curve along the time axis, and the melt end date in every year is the last sharp rising edge for the backscatter coefficient curve along the time axis, and melt duration can been obtained by the sum of each period of the year. The method can detect whether each pixel experiences freezing and thawing and determine freeze-thaw time. The basic steps of the algorithm are as follows:

(1) Preprocess long time series of backscatter coefficient data.
(2) Mathematical morphology does the filtering for the preprocessed long time series of backscatter coefficient data.
(3) Use wavelet transform for long time series of backscatter coefficient data processed by mathematical morphology to do the multi-scale wavelet decomposition and extract the edge information under different scales.
(4) Automatically obtain the optimal edge threshold of wet snow and dry snow classification by using variance analysis and generalized Gauss model based on the extracted edge in step (3) .
(5) Obtain the distribution map of Antarctic snowmelt onset date, duration and end date of each pixel based on the optimal edge in step (4).

(6) Design a median difference operator to automatically check and flag potential errors. We examined each pixel with 3×3 neighbourhood, which ultimately determines the melt onset date, melt duration and melt end date.

Results and Discussion

Antarctic microwave scatterometer QuikSCAT data from July 1, 2000 to June 30, 2001 is used to study the snowmelt information, and the long time series of the backscatter coefficient data is done by preprocessing method to eliminate the problem data, and then partial external interference can been removed by edge-preserving mathematical morphology. Automatically obtain the optimal classification threshold of dry snow and wet snow through the wavelet edge detection and the generalized Gauss mode, and then obtain the Antarctic snowmelt distribution map. Figure 3 is distribution map of the Antarctic melt onset date, duration and end date from July 1, 2000 to June 30, 2001 based on mathematical morphology combined with wavelet transform. Figure 4 is distribution map of the Antarctic melt onset date, duration and end date from July 1, 2000 to June 30, 2001 based on wavelet transform.

The total melt areas of Figure 3 are about 902,499 square kilometres, accounting for 6.5 % of the total Antarctica. The total melt areas of Figure 4 are about 998,046 square kilometres, accounting for 7.2 % of

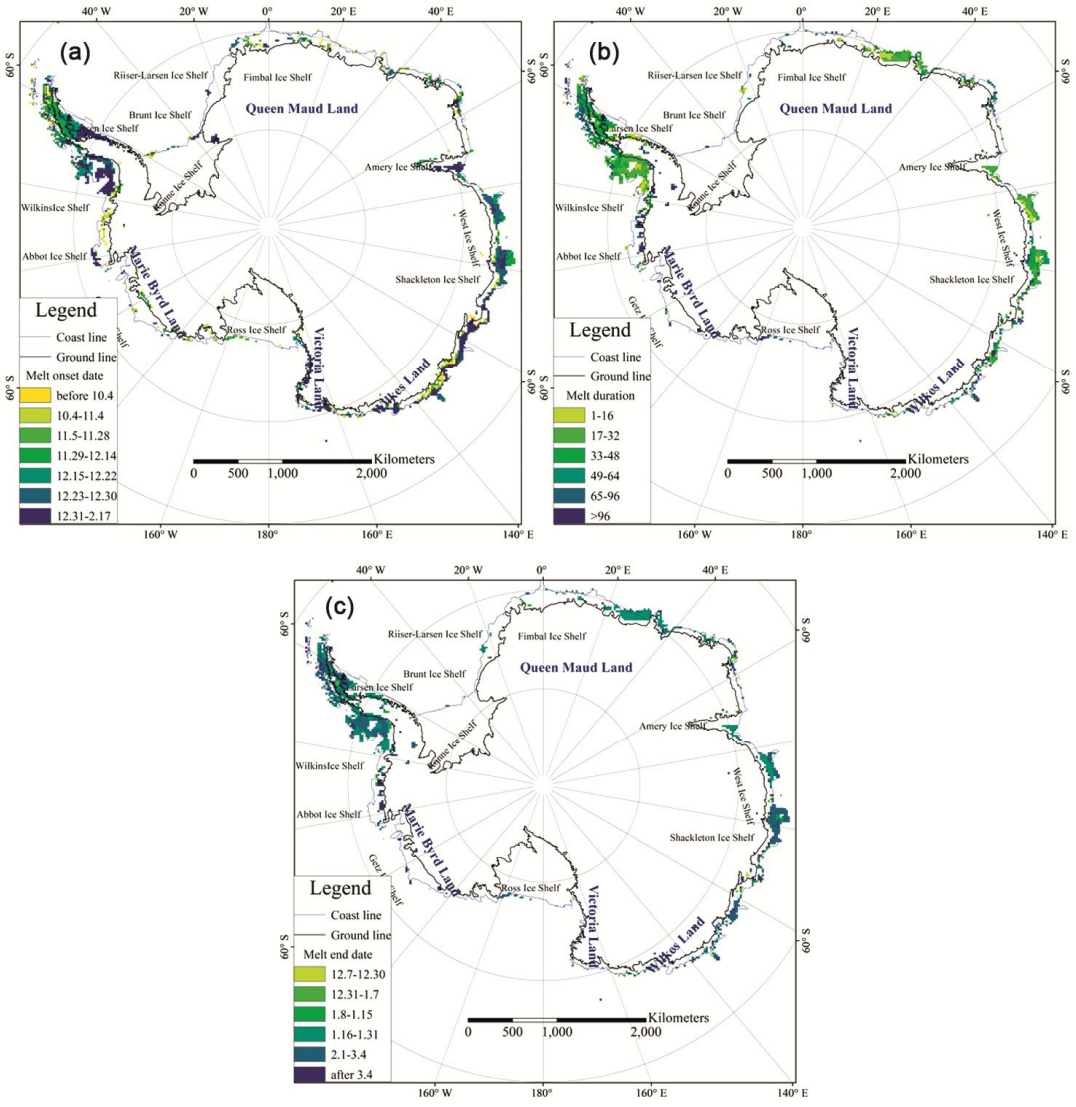

Fig. 3 — Antarctic snowmelt detection results based on edge detection for scatterometer data for the proposed method (a) Melt onset date (where, 10.4 is October 4, 2000, and so on) (b) Melt duration (c) Melt end date

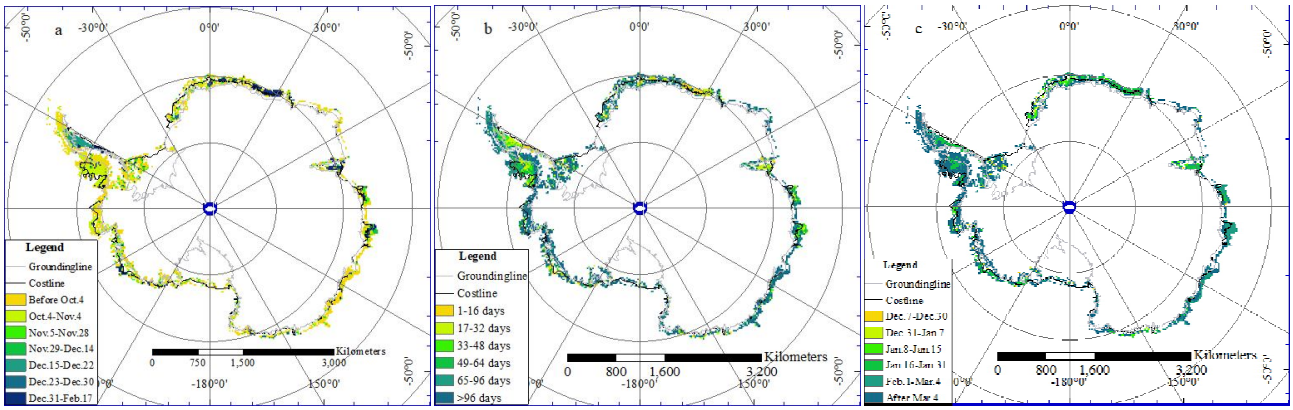

Fig. 4 — Antarctic snowmelt detection results based on edge detection for scatterometer data for wavelet transform method (a) Melt onset date (where, 10.4 is October 4, 2000, and so on) (b) Melt duration (c) Melt end date

the total Antarctica. We can see from Figure 3 and Figure 4 that the melt areas were mainly distributed on the edge of the Antarctic ice shelves and there are many differences in melt onset date, duration and end date.

Use the near surface air temperature data of ten automatic weather stations from July 1, 2000 to June 30, 2001 to verify melting state of wet snow and dry snow, and the geographic information of ten automatic weather stations are shown in Table 1, and the temperature variation curve of the dry snow stations is shown in Figure 5 and the temperature variation curve of the wet snow stations is shown in Figure 6.

From Figure 5, the air temperatures of six dry snow sites change greatly from July 1, 2000 to June 30, 2001, but the annual air temperatures are lower than -5 °C , which indicates that the locations of six automatic meteorological stations were not melt, and this is consistent with the ice-sheet freeze-thaw detection results obtained by the proposed algorithm as shown in Figure 3.

As we can see in Figure 6, Butler Island station reached 0 °C or more than 0 °C only in early January and mid January, which is very consistent with the results shown in Figure 3. The air temperatures in Larsen Ice Shelf station and Cape Denison station reached 0 °C or more than 0 °C in mid December, and the air temperatures began less than 0 °C in February, and the ice-sheet freeze-thaw detection results are consistent with the results of these two sites. Bonaparte Point station location is in the melt state from November 2000 to the end of March 2001, which is very consistent with the air temperature results shown in Figure 6.

Table 1 — Geographic information of ten automatic weather stations

Type	Name	Code	Longitude	Latitude
Dry snow points	Swithinbank	356	81.20˚S	126.17˚W
	Elizabeth	361	137.08˚W	82.61˚S
	Harry	900	121.39˚W	83.00˚S
	Relay Station	918	43.06˚E	74.02˚S
	Siple Dome	938	148.77˚W	81.66˚S
	Dome C II	989	123.37˚E	75.12˚S
Wet snow points	Butler Island	902	60.16˚W	72.21˚S
	Bonaparte Point	923	64.07˚W	64.78˚S
	Larsen Ice Shelf	926	60.91˚W	66.95˚S
	988	988	142.66˚E	67.01˚S

It can been seen that the snowmelt results based on mathematical morphology combined with wavelet edge detection algorithm can accurately reflect the Antarctic snowmelt time and space distribution by the comparisons of the air temperatures of 10 typical dry and wet snow sites and the results of the proposed method.

In order to verify the feasibility of mathematical morphology combined with wavelet transform, the results are compared with wavelet transform method. It can been seen from Figure 6 that the temperature of Cape Denison is higher than 0 °C for 32 days. Nevertheless, the melt duration of wavelet transform method is 16 days, and the melt duration of the proposed method is 20 days, so the detection accuracy is about 50 % for the wavelet transform method and the detection accuracy is about 62.5 % for the the proposed mathematical morphology combined with wavelet edge detection method. Overall, the proposed method has more accurate.

In short, the proposed mathematical morphology combined with wavelet edge detection algorithm can

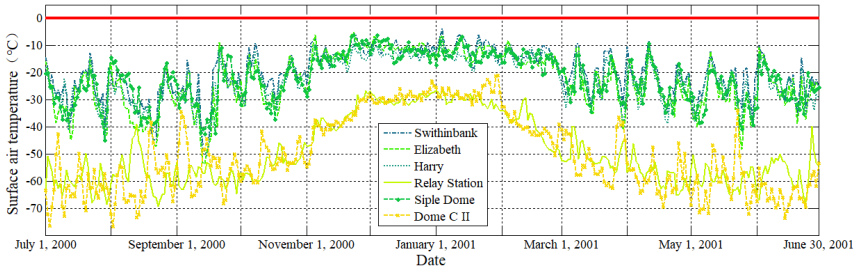

Fig. 5 — Temperature change of Antarctic dry snow sites

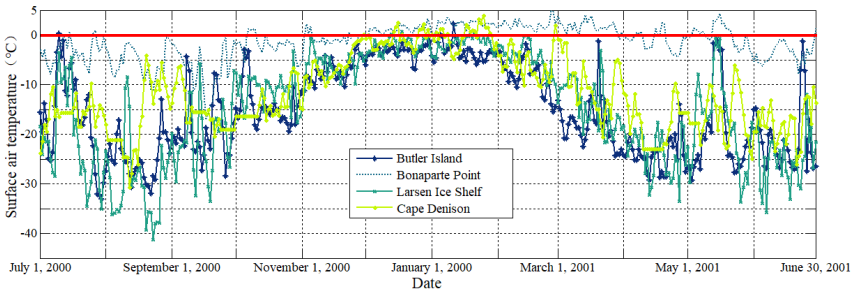

Fig. 6 — Temperature change of Antarctic wet snow sites

not only extend ice-sheet freeze-thaw detection method of the microwave scatterometer, but also obtains better snowmelt detection results.

Conclusion

The backscatter coefficient of microwave scatterometer is very sensitive to the liquid water content of the snow. With melting begins and ends, the backscatter coefficients will have dramatic changes, and a new automatic Antarctic snowmelt detection method was proposed based on microwave scatterometer SeaWinds/QSCAT data by mathematical morphology combined with wavelet transform. The method did not depend on the priori snowmelt information. To some extent, this method can improve the snowmelt detection accuracy because this method can remove most of the interference by the filtering of mathematical morphology. Comparison of the freeze-thaw results in this work with the surface air temperature of ten automatic weather stations shows that the proposed snowmelt detection method is feasible.

Acknowledgement

This research was supported by Open fund project of National-Local Joint Engineering Laboratory on Digital Preservation and Innovative Technologies for the Culture of Traditional Villages and Towns (No. CTCZ18K07), Key Laboratory of Ocean Circulation and Waves, Institute of Oceanography, Chinese Academy of Sciences (No.KLOCW1805).

References

1 Wang, L., Deriving spatially varying thresholds for real-time snowmelt detection from space-borne passive microwave observations. *Remote Sens. Lett.*, 3 (2012) 305-313.

2 Zwally, H.J., & Fiegles, S., Extent and Duration of Antarctic Surface Melting. *J. Glaciol*.., 40 (1994) 463-476.

3 Oza, S., R., Spatial-temporal patterns of surface melting observed over Antarctic ice shelves using scatterometer data. *Antarc. Sci*., 27 (2015) 403-410.

4 Wismann, V., Monitoring of seasonal snowmelt on Greenland with ERS scatterometer data. *IEEE T. Geosci. Remote*, 38 (2000) 1821-1826.

5 Wang, X.D., Li, X.W., Wang, C. & Li, X.G., Antarctic ice-sheet near-surface snowmelt detection based on the synergy of SSM/I data and QuikSCAT data. *Geosci. Front.*, 9 (2018) 955-963.

6 Bothale, R.V., Rao, P.V.N., Dutt, C.B.S., Dadhwal, V.K., Maurya, D., Spatio-temporal dynamics of surface melting over Antarctica using OSCAT and QuikSCAT scatterometer data (2001-2014). *Curr. Sci.* , 109 (2015) 733-744.

7 Bothale, R.V., Rao, P.V.N., Dutt, C.B.S., Dadhwal, V.K., Detection of snow melt and freezing in Himalaya using OSCAT data. *J. Earth Syst. Sci*., 124 (2015) 101-113.

8 Steiner, N. and Tedesco, M., A wavelet melt detection algorithm applied to enhanced-resolution scatterometer data over Antarctica (2000-2009). *Cryosphere*, 8 (2014) 25-40.

9 Semmens, K.A., Ramage, J., Bartsch, A., Liston, G.E., Early snowmelt events: detection, distribution, and significance in a major sub-arctic watershed. *Environ. Res. Lett.*, 8 (2013) DOI: 10.1088/1748-9326/8/1/014020.

10 Nghiem, S.V., Steffen, K., Neumann, G., Huff, R., Mapping of ice layer extent and snow accumulation in the Percolation Zone of the Greenland ice sheet. *J. Geophys. Res.Earth.*, 110 (2005) DOI: 10.1029/2004JF000234.

11 Wang, L., Derksen, C., Brown, R., Detection of Pan-Arctic terrestrial snowmelt from QuikSCAT, 2000-2005. *Remote Sens. Environ*., 112 (2008) 3794-3805.

12 Wang, L., Sharp, M., Rivard, B., Steffen, K., Melt season duration and ice layer formation on the Greenland ice sheet, 2000-2004. *J. Geophys. Res.Earth*., 112 (2007) F04013, DOI: 10.1029/2007JF000760.

13 Drinkwater, M.R., Long, D.G., Bingham, A.W., Greenland snow accumulation estimates from satellite Radar scatterometer data. *J Geophys. Res*., 106 (2001) 33935-33950.

14 Sharp, M., Wang, L., A five-year record of summer melt on Eurasian Arctic ice caps. *J. Climate*, 22 (2009) 33-45.

15 Ashcraft, I.S., Long, D.G., Comparison of methods for melt detection over Greenland using active and passive microwave measurements. *Int. J. Remote Sens*., 27 (2006) 2469-2488.

16 Ashcraft, I.S., Long, D.G., Sea Winds views Greenland. *In Proceedings of the IEEE International Geo Science and Remote Sensing Symposium*, 3 (2000) 1131-1136.

17 Nghiem, S.V., Steffen, K., Kwok, R., Tsai, W.Y., Detection of snowmelt regions on the Greenland ice sheet using diurnal backscatter change. *J. Glaciol*., 47 (2001) 539-547.

18 Bartsch, A., Kidd, R..A., Wagner, W., Bartalis, Z., Temporal and spatial variability of the beginning and end of daily spring freeze/thaw cycles derived from scatterometer data. *Remote Sens. Environ*., 106 (2007) 360-374.

19 Brown, R., Derksen, C., Wang, L., Assessment of Spring Snow Cover Duration Variability over Northern Canada from Satellite Dataset. *Remote Sens. Environ*., 111 (2007), 367-381.

20 Oza, S.R., Singh, R.K.K., Vyas, N.K., Sarkar, A., Study of Inter-annual Variations in Surface Melting over Amery Ice Shelf, East Antarctica, Using Space-borne Scatterometer Data. *J. Earth Syst. Sci*., 120 (2011) 329-336.

21 Sharifi, K. and Leon-Garcia, A., Estimation of shape parameter for generalized Gaussian distributions in subband decomposition of video. *IEEE T. Circ. Syst. Vid.*, 5 (1995) 52-56.

22 Dupont, F., Royer, A., Langlois, A., Gressent, A., Picard, G., Fily, M., Cliche, P., Chum, M., Monitoring the melt season length of the Barnes Ice Cap over the 1979-2010 period using active and passive microwave remote sensing data. *Hydrol. Process*., 26 (2012) 2643-2652.